applied sciences

MDPI

Article

Insights on Niobium Micro-Alloyed Laser In Situ Synthesised Gamma Titanium Aluminide Alloys

Monnamme Tlotleng [1,2,*], Sisa Pityana [1] and Sibusisiwe Motha [3]

[1] Laser Enabled Manufacturing Group, Photonics Centre, Council for Scientific and Industrial Research, Pretoria 0001, South Africa
[2] Department of Mechanical Engineering Science, Faculty of Engineering and the Built Environment, University of Johannesburg, Auckland Park Campus, Johannesburg 2006, South Africa
[3] School of Chemical and Metallurgical Engineering, University of the Witwatersrand, 1 Jan Smuts Avenue, Johannesburg 2050, South Africa
* Correspondence: mtlotleng@csir.co.za; Tel.: +27-12-841-2395

Abstract: The effects of micro-alloying gamma titanium aluminide (γ-TiAl) with niobium (Nb) using a laser melt pool as a melting pot are reported. The Optomec LENS machine was used to carry out the laser in situ alloying experiments where Nb, ranging from 6 to 10 (at. %), was added to the stable binary γ-TiAl alloy. The results of this study concluded that when a stable binary γ-TiAl alloy is micro-alloyed with Nb, there is a definite microstructural transformation, anneal twinning, promotion, and retardation of aluminium solubility in the dual and pure γ phases, respectively. Twinning in the as-built in situ alloyed ternary Ti–48Al–xNb was for the first time reported in this study. It was observed that 6 at. % Nb promoted twinning in the as-built sample, which inferred that the sample might have room temperature ductility. In fact, it was shown that the twins formed in the as-built sample dissipated with the addition of Nb. A heat treatment temperature of 1200 °C promoted anneal twinning only in the binary alloy, as confirmed by XRD data. Meanwhile, this twinning was absent in all the ternary alloys when they were heat treated to a temperature of 1200 °C. Anneal twinning was confirmed only for the alloy containing 8 Nb (at. %) at 1400 °C. Stalk faults, dislocations, and dislocation pile-ups were observed in the α_2 phase of the alloys. Aluminium solubility was seen to increase in the $\alpha_2 + \gamma$ (±49 at. %) phase alloy and sharply decrease in the pure γ (>49 at. %) phase alloys. Most importantly, this study determined that the laser in situ alloying process was highly exothermic. The heat gained by the reaction was found to increase with the increase in niobium content.

Keywords: aluminium; anneal twinning; gamma titanium aluminides; heat treatment; laser in situ alloying; niobium

Citation: Tlotleng, M.; Pityana, S.; Motha, S. Insights on Niobium Micro-Alloyed Laser In Situ Synthesised Gamma Titanium Aluminide Alloys. *Appl. Sci.* **2023**, *13*, 5725. https://doi.org/10.3390/app13095725

Academic Editor: Antonio Miotello

Received: 28 February 2023
Revised: 24 April 2023
Accepted: 28 April 2023
Published: 6 May 2023

1. Introduction

Additive manufacturing (AM), also commonly known as 3D printing, is unlike subtractive methods since complex parts are produced additively layer by layer relying on a computer-aided device (CAD) file [1,2]. During printing, the feedstock, i.e., powder or wire or a combination-off, is irradiated with an energy source either fully or partially until a desired part is complete. Distinctively, a laser beam or electrons are used as an energy source leading to AM techniques being classified as either laser AM or electron beam AM platform. In addition, a platform can be classified as either powder bed (PB) or direct energy deposition (DED); depending on how the feedstock is handled, fed, and interact with the energy source during deposition. Electron beam melting (EBM) and selective laser melting (SLM) are classified as powder bed platforms since the powder is overlaid on the depositing bed, typically a metal slab, before being irradiated and fused into the desired part. During DED powder is injected into a melt pool; that is created on the base plates, and upon solidification it fuses into a desired part. The significant difference between

PB and DED system is in the complexity of structures that can be printed and the energy inputs that the built part can experience during manufacturing. DED is sustained with high energy inputs and temperature gradients that are due to the remelting of the previously deposited layer when compared to SLM systems. Hence parts which are 3D printed with DED systems are typically in-homogenous, microstructurally somewhat tempered, and highly stressed due to the thermal cycles that are experienced during manufacturing [3]. During process development most of the powder flow rates, laser spot size, laser-powder spot interaction (concentricity) are optimized to prevent powder inefficiencies, the loss in built edges, tearing, and rough surface finish.

There are several DED systems, and these include direct metal deposition (DMD), direct laser metal deposition (DLMD), laser metal deposition (LMD), laser cladding (LC), and others. The Optomec 850-R LENS DED platform was used to carry out the aim and objectives of this research work. The aim was to investigate whether the 850-R LENS can be instrumental in printing ternary titanium–aluminium–niobium alloys from single-phase elemental powders as feedstock. The importance of this study was to help in elucidating and articulating the effects of niobium (Nb) on the composition (in-flight tweaking), microstructural transformation, and twinning of the gamma titanium aluminide alloys. This would be beneficial in understanding metallic alloying from the perspective of laser "in situ" alloying and begin to adapt the available powder metallurgy phase diagrams for laser-based 3D printed alloys from the elemental powder as opposed to pre-alloyed powders. The 850-R Optomec LENS is unique to other DED platforms since it offers freedom of operation. The 850-R LENS features include multiple hoppers that can be controlled simultaneously or independently (using software) and has an additional rotational and tilt movement that complete its five-axis movement during printing. The platform consists of three cameras, thermal sensor, and a pyrometer that are useful in melt-pool dynamics studies. Most recently, Researchers at the Council for Scientific and Industrial Research, South Africa, have demonstrated that at most four external hoppers and a substrate heating source can be integrated and feature as part of the LENS during processing. This therefore makes the 850-R LENS at the CSIR, South Africa a multiple hopper and heat-controlled platform in contrast to other 3D printers such as the Arcam EBM Spectra H, which is a powder bed system and commercially available and costly.

Contrast to PB systems, the 850-R LENS can print metal structures from single-phase powder (e.g., Ti), pre-alloyed powder (e.g., Ti64), functionally graded structures (e.g., Ti: Ti64), composites (e.g., Ti–HAp), and reinforcements (e.g., WC–Ti). Recently, there are studies that develop in situ alloyed metallic structures from either elemental powders, and metallic powder and wire as feedstock. This research method is a development towards tailored microstructures and intended applications for structures with improved properties which can adapt and have memories. This field of research (laser alloy development) is new and in its infancy, however, it is receiving tremendous attention given its economic benefits and freedom of manufacturing [4]. From limited published literature studies, R&D on alloy development by means of laser, as a heat source, are concerned mainly with reactive synthesis of intermetallic alloys including titanium aluminides (Ti–Al) for aerospace, energy, and automotive industries; Nitinols (Ni–Ti) for biomedical industry and high entropy alloys for electronics; and research studies that are concerned with the characteristics of the melt pool and its dynamics (thermal and kinetics). The benefit from these studies would evolve a system that is able to 3D print crack sensitive alloys such as Ti–Al, Ni–Ti, and high entropy alloys which are currently found to be difficult to manufacture into components with traditional methods including certain 3D printing platforms. Arcam EBM Spectral H is a revolutionary machine that can 3D print crack-free, stress relieved components with improved material properties such as wrought and better than cast. This machine takes into consideration all the requirements for 3D printing crack-sensitive alloys. This Arcam machinery uses multiple beams as a beam source, and processing occurs inside a vacuum at high temperature. Ti–Al rotor blades that were 3D printed using this machine have undergone testing and will go into the GEnx and GE9X for

Boeing's Dreamliner 747-8 aircraft and Boeing's next-generation long-haul plane (The 777X), respectively. This achievement solves the machine aspects of printing Ti–Al alloys but does not account for the aspect of in situ alloying that would be necessary for alloy tweaking, microstructural tailoring, and building of smart functional parts that are adaptive. To engineer such structures, DED machines are best suited since alloying using PB platforms is still not understood, or it is not a straightforward process. DED has advantages since it can feed both elemental powders, wires, and a combination of these feedstocks [5].

Ti–Al alloys are regarded as the best aeronautical structural materials due to their lightweight and extensive thermo-mechanical properties. The United State Patent no 5,415,831, dated 16 May 1995, revised the following: "alloys based on doped intermetallics are acquiring increasing importance in materials technology. This is because doped intermetallics, particularly aluminides, possess high strength regardless of their low density". Gamma (γ) Ti–Al is superior, in specific strength, to nickel (Ni) base super-alloys at temperatures of about 800–900 °C, but they have limited room temperature ductility, and are sensitive to process selection and conditions [6–9]. Despite these observations, General Electric (GE) Ti–48Al–2Nb–2Cr or 48–2–2 alloy has been reported to have commercial use in the GEnx-family engines produced by GE Aircraft Engines [3,10]. To date, this is the most successfully researched, developed, and commercialized alloy, followed by the Helmholtz Association of German Research Centres (GKSS, Germany) Ti–48Al–9Nb alloy, which is commercially unavailable. The Ti–48Al–9Nb alloy is mainly used for manufacturing parts that are used in high temperature applications, whereas 48–2–2, in addition to being a high temperature application alloy, has to some degree room temperature ductility [11]. There are several studies that have reported the required process setting to achieve crack-free parts manufactured from commercially available Ti–Al alloys. Clemens et al. [12] HIPped a cast γ-TiAl sample and were able to refine the microstructure, reduce lamellar spacing to 30–40 nm, and hardness significantly to a point of improved ductility. While this method is successful, it highly costly to implement. AM techniques are being investigated to achieve superior Ti–Al parts, but for this to happen it would mean the current platforms have to be reconfigured or adapted to meet the required Ti–Al process conditions. Adaptation would involve incorporation of heating elements on the platform and systems' surrounding, thermo-kinetics monitoring optics and cameras, and a control software for temperature manipulation, and laser control. Most importantly pre-heating of the powders before deposition will be a necessity.

The ability of feeding multiple powders during printing can lead to a decrease in material use and cost-effective manufacturing route while achieving smart functional parts. Gasper et al. [4] concluded that laser in situ alloying synthetic approach can lead to 40% of material cost reduction in relation to use of pre-alloyed powder through studying the synthesis of the GE 48–2–2 alloy. Shishkovsky et al. [5] reported FGMs of Ti–Al and concluded that hardness could be controlled by changing powder composition using the appropriate CAD model. Notably R&D towards understanding the practical studies of laser in situ alloying and manufacturing could be costly since powder that is generated during developmental studies might not be in equilibrium or mimic any alloy with significant metallurgical use; in which case the powders would have to undergo further powder processing to be used for AM. To avoid excess powders being generated during the developmental studies, we propose that fundamentals studies be preceded with the understanding of mass calibrations where mass balance charts are generated. Standard procedure would include understanding the effect of carrier and shrouding gas flow-rates and feed speed (rotational per minute or rpm) powder mixing, first, and then mixing during laser alloying.

This paper looks at using the Optomec LENS machine for studying the synthesis of a ternary alloy containing Ti–Al–Nb. During synthesis, the effects of Nb on the microstructure evolution, dissolution of Al in the γ-rich phase Ti–Al alloy and twinning in the as-built state will be studied, followed with effects of heat-treatment and twinning in the annealed condition(s). TNB/TNM alloys are the Ti–Al alloy system that contain Nb or molybdenum (Mo) and are important to aerospace companies due to their mechanical properties, in

particular machinability, and use in high temperature conditions. TNB/TNM alloys have improved ductility, in the cast lamellar state, at room temperature [3]. Ti–Al–Nb has several phases (α_2, γ, σ and β) that form during synthesis. Typically, the α_2 + γ phase Ti–Al alloys are used in the compressor and low temperature turbine blades of the jet engines. Therefore, by adding niobium to this stable phase, a γ-TiAl and σ-Nb_2Al lower temperature microstructure is formed with a possibility of an improved high temperature alloy containing the β phase resulting. According to Kesler et al. [13], the σ-Nb_2Al phase is hard and brittle and cannot promote any material ductility at elevated temperature even when toughened by a ductile second phase. Yoshihara and Miura [14] concluded that oxidation resistant of γ-TiAl alloys can be achieved by adding about 1–10 Nb (at. %). Alloys containing 5–10 Nb (at. %) are desired for high-temperature applications. Hashimoto et al. [15] studied the effects of third element on binary Ti–Al and concluded that by adding large amount of niobium to a stable Ti48Al (at. %) alloy, one can improve ductility of a gamma (γ) single-phase alloy. They further summarized that ductility of the Ti–Al alloy can be improved by producing fine microstructure, increasing anneal twinning in the γ-phase, decreasing the α_2 phase, and decreasing Al content in the γ-phase. These effects depend on the amount of niobium being added to a stable binary Ti–Al phase. Kawabata et al. [16] reviewed that room temperature ductility of Ti–48Al (at. %) can be improved by adding chromium, vanadium, molybdenum, and manganese and showed that 2 (at. %) of niobium result in a small increase in yield and fracture stresses, and large increase of fracture strain at 873 K (599.85 °C). In this paper, 6–10 (at. %) of niobium was added to the stable Ti–48Al (at. %) alloy to study the effect of niobium in microstructural transformation, anneal twinning, and heat treatment.

2. Materials and Methods

2.1. Materials

Pure Ti, Al, and Nb were used as feedstocks in this study. Both Ti and Al powders were spherical and had a particle size distribution ranging from 45 to 90 µm. The two spherical powders were supplied by TLS Technik (Bitterfeld, Germany), while Nb, which was irregular in shape, was supplied by Weartech (Johannesburg, South Africa). The morphology and elemental composition of the ternary powders are shown in Figure 1. Irregular and oval-like particles represent Nb powder, while the bright spherical particles are Al and the greyish spherical powder particles are Ti. Chemical analyses show that the powders had different compositions.

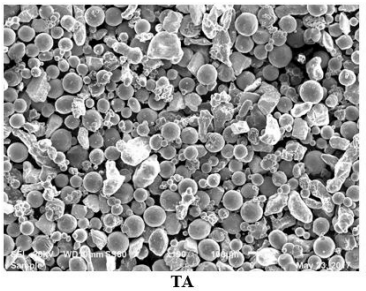

TA

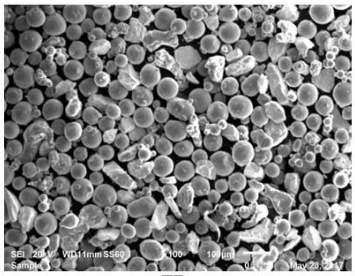

TB

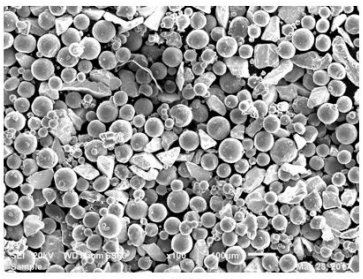

TC

Powder composition

Element (at. %)	TA	TB	TC
Al	77.00	53.00	46.00
Ti	19.10	41.71	45.20
Nb	3.46	5.77	9.30

Figure 1. Powder distribution and composition before processing.

2.2. Methods

2.2.1. Laser Metal Deposition

The 850-R Optomec LENS machine was used to manufacture Ti–Al–Nb test coupons. This manufacturing platform uses a 1000 W IPG fibre laser that is connected to the deposition head. The LENS used a powder deposition head that was made of steel, while the nozzles were manufactured out of brass. The set-up allowed for the laser beam and depositing powder to be concentric and controlled simultaneously during deposition. The process of 3D printing is controlled automatically using the Workstation Control Software, version 3.1.10. The schematic set-up is shown in Figure 2.

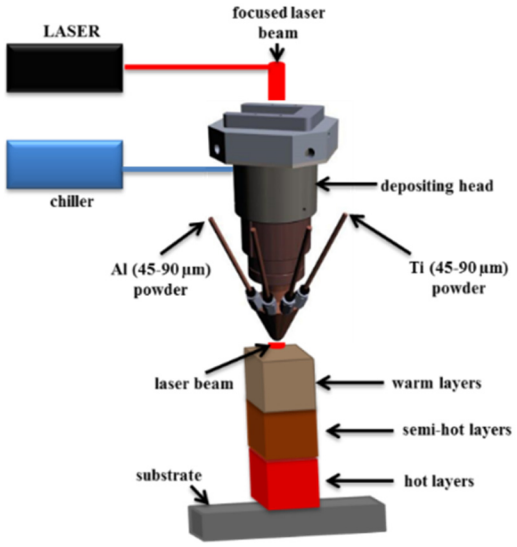

Figure 2. Schematic representation of the LENS set-up.

The set-up shows only two hoppers for manufacturing. Ti and Nb were feed from the same carrier gas line but in different hoppers. Nb is deposited from an external hopper manufactured and supplied by GVN. Table 1 reports the process parameters that were used to manufacture the Ti–Al–Nb coupons that were studied in this paper.

Table 1. DED process parameters.

Parameter	Symbol	Set-Value	Unit
Laser power	P	800	W
Laser spot size	D	1.4	mm
Deposition speed	S	20.8	in/min
Laser Energy Density	Eρ	40.58–81.17	J/mm^2
Powder Mass (BA)	M	2.67	g
Powder Mass (TA)	M	1.72	g
Powder Mass (TB)	M	1.66	g
Powder Mass (TC)	M	1.31	g

Powders were deposited onto Ti–6Al–4V substrates with dimensions of 140 × 140 × 7 mm^3. A cube sample with dimensions of 20 × 20 × 5 mm^3 was produced using optimised laser deposition parameters for each alloy. Post-manufacturing of the samples, still on the base plate, involved cutting them into 4 pieces of 5 mm each (control sample, as-built sample, and heat treatment samples) for heat treatment and characterisation.

2.2.2. Heat Treatment

Heat treatment is regarded as the post-processing method by which the microstructure of the as-built laser samples can be homogenised while relieving them of internal stress.

According to the Ti–Al binary phase diagram, different heat treatment temperatures can be used to produce different microstructures containing different amounts of Al. This is dependent on the method of cooling and the alloy composition (Al content). The microstructural evolution and phase transformation of Ti–Al alloys are reported by Kothari et al. [17]. In this paper, heat treatment was conducted using a Carbolite tube furnace in an argon-rich environment. The samples were heated to temperatures of 1200 °C and 1400 °C, respectively, before furnace cooling. Temperature was ramped at 20 °C/min from room temperature to the set temperature and held for 2 h before furnace cooling. Heat treatment details are summarised in Table 2.

Table 2. Heat treatment conditions.

Sample ID	Temperature (°C)	Holding Time (min)	Method of Cooling
As-built	25	None	None
HT 1	1200	120	Furnace cooling
HT 2	1400	120	Furnace cooling

2.2.3. Sample Preparation and Characterisation

Ti–Al–Nb samples were prepared for metallographic observations and characterisation. The samples were mounted in a carbon-black resin and polished with OP-S suspension to a 0.04-micron surface finish using the Struers TegrsForce-5 auto/manual polisher. The samples were then etched by immersing into Krolls' reagent. Olympus BX51M that uses SC30 camera was used for microstructural visualization, while Joel's JSM-6010Plus/LAM scanning electron microscopy (SEM) that was equipped with energy dispersive X-ray was used for microstructural and chemical composition analyses. Phase analysis was conducted using the X'Pert PANalytical X-ray diffraction machine that used a Cu source. During data acquisition, the Cu source was excited with a current and voltage of 40 mA and 54 kV, respectively. The source was scanned at a step size of 0.04° within a 2θ range of 10° to 100°.

3. Results

Figure 3 presents the microstructure of the as-built and heat-treated binary Ti–Al alloy.

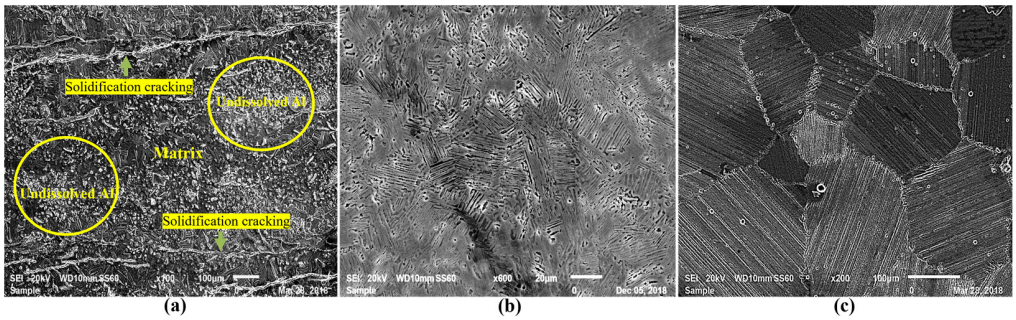

Figure 3. LENS synthesised Ti–Al: as-built (**a**), HT 1200 °C (**b**), and HT 1400 °C (**c**).

The elemental analyses of the as-built (or produced) alloy and subsequent heat treatments (1200 °C and 1400 °C) concluded that the as-built binary Ti–Al alloy contained 76 (at. %) Ti and 24 (at. %) Al. After heat treatment at 1200 °C, aluminium increased to 49 (at. %), while Ti decreased to 51 (at. %). There was no significant change in chemistry when the sample was heat treated to 1400 °C, since 52 (at. %) Ti and 48 (at. %) Al were reported. The difference in the chemistry between the as-built and heat-treated samples was attributed to the dissolution of the free aluminium, which tends to bubble out of melt-pool solution, and its segregation during laser in situ alloy synthesis. The segregated aluminium can be said to be the cloud or white and bright material/phase that sits on the matrix of the alloy and is wrapped as a filler in the formed solidification cracks, as seen from Figure 3a. Post-heat treatment led to an equiaxed lamellae microstructure (Figure 3c) and a duplex

phase microstructure (Figure 3b) being formed. These microstructures are further discussed in the latter sections of this paper under anneal conditions. These microstructures have limited engineering applications. To improve their odds of having industrial applications, researchers' micro-alloy the stable binary γ-TiAl with stabilising metals such as chromium (Cr) and niobium (Nb). Herein, ternary alloys containing Nb were fabricated and are reported in Figure 4.

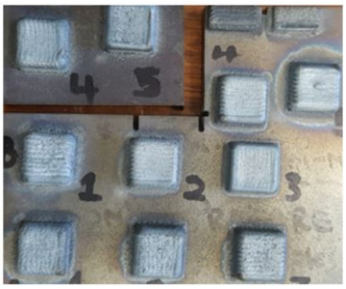

Figure 4. As produced coupons of Ti–Al–Nb.

Figure 4 shows printed cubes that look different considering their surface texture. The surface texture or finish of the ternary cubes looks smooth to rough, but not as rough as the surface of the binary Ti–Al alloy. The surface smoothness was observed to increase with the increase in niobium feed rate (rpm), as seen with cube 1 (which corresponds to 1.0 rpm), cube 2 (which corresponds to 1.6 rpm), and cube 3 (which corresponds to 2.0 rpm), respectively. More importantly, as opposed to the binary alloy, the ternary cubes were produced with no obvious surface cracks. It was anticipated from working with the binary alloy (Ti–Al) that the ternary alloys would have massive surface cracks or even delaminate. Intense cracking is attributed mainly to rapid melt-pool heating and cooling rates during printing or the inherent residual stresses and brittle nature of aluminides.

The absence of surface cracks in the ternary builds could not be explained immediately. Balichakra et al. [18] studied the laser surface melting of γ-TiAl alloy, both experimentally and numerically, by varying the laser power. They observed micro-cracking in the melted region of the built, which was due to rapid cooling rates, and concluded that these high cooling rates led to refined microstructures. Kenel et al. [19] reported a curve showing the cracking frequency with an increase in energy input and concluded that cracks decreased with the increase in energy input. During LENS printing of the ternary cubes (being studied here), the brightness and glow of the melt pool were seen to increase with the increase in the niobium content. Intuitively, this meant that the melt-pool thermal heat, or temperature, was increasing with an increase in niobium content. The increase in the melt-pool temperature or thermal heat led to the inference that the process of doping binary Ti–Al with niobium was "endothermic", and this might be an explanation for the absence of surface cracks and surface smoothing with the increase in niobium. The "endothermic" nature of the reaction would mean that the process of making Ti–48Al–xNb was sustained with slow cooling rates when compared to the synthesis of the binary Ti–48Al. This inference supports the observations by Kenel et al. [19] and Balichakra et al. [18] (on cracking). The microstructures of the ternary alloy before heat treatment are reported in Figure 5, with the corresponding chemical composition reported in Table 3. Table 3 shows that three ternary alloys (TA, TB, and TC) were achieved.

Table 3 illustrates that niobium content was seen to be decreasing with the increase in rpm. From Table 3, it is seen that the solubility of aluminium in the alloy increased with the decrease in niobium and titanium, respectively. Niobium is regarded as a micro-alloying element with the potential to improve processability and solid solution strengthening of the γ-phase Ti–Al alloys while modifying their deformation mechanism. The microstructures of the alloys are reported in Figure 5.

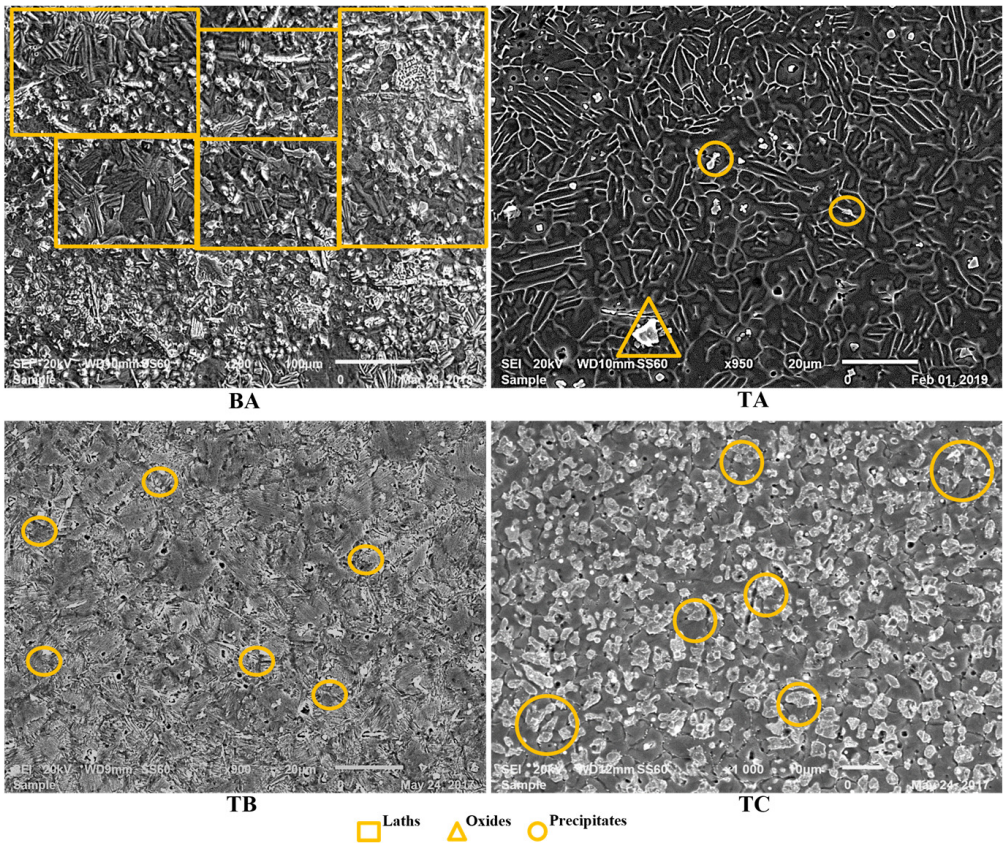

Figure 5. Microstructures of the as-built Ti–Al/Nb alloys.

Table 3. Chemical composition of the alloys.

ID	Ti	Al	Nb
BA	75.94 (76)	24.06 (24)	0.00
TA	43.93 (44)	45.93 (46)	10.15 (10)
TB	33.80 (34)	58.03 (58)	8.17 (8)
TC	27.82 (28)	65.86 (66)	6.33 (6)

Note that the numbers in brackets are whole numbers of the actual EDS.

SEM micrographs reported in Figure 5 compare the binary alloy to its ternary alloys before heat treatment. Figure 5 indicates that when niobium was added to the Ti48Al (at. %) alloy, it had a tremendous effect on the resulting microstructure in the as-built state. The binary alloy (BA) microstructure was predominantly $\alpha_2 + \gamma$ with thick laths or agglomerated α_2 lamellae structures that seemed to form precipitates as indicated on the image. This observation suggests that α_2 lamellae structure has a different density and melting temperature than that of the γ rich phases. The bright white fields that are present can be interpreted as aluminium-rich islands, concluding that the binary alloy was heterogeneous. The immediate microstructural transformation with the addition of niobium can be deduced from Figure 5, as seen from the microstructures labelled TA, TB, and TC.

It was observed that 6 (at. %) of niobium transformed the previously formed α_2 thick laths into a $\gamma + \alpha_2$ microstructure that contained β-precipitate (TC). The 8 (at. %) niobium transformed the previously formed thick laths into lamellae-grained microstructure with some β-precipitate (o) (TB), and finally, the, 10 (at. %) niobium would lead to a full dissolution of the previously formed laths into fine α_2/γ lamellar structure, with the observed α_2 lamellar structures serving as grain boundaries within which γ phase was contained. Some of the oxides (o) and β-precipitate (o) could still be observed (TA). Chemical analyses conducted on the observed bright white precipitates concluded that this

was an alumina (Al_2O_3) phase. This oxide phase improves the high-temperature oxidation and creep properties of these alloys. Yoshihara and Miura [14] reported that niobium of up to 10% (at.) can promote the oxidation resistance of the TiAl alloys. The observed microstructural transformation, with the addition of niobium content, can be summarised as follows: thick lamellar → β-precipitates → α_2 + γ grain formation → fine lamellar structure. A lamellar microstructure is more ductile than an equiaxed microstructure. The results here concluded that TA alloy would be ductile and have improved creep properties in the as-built state.

To understand this microstructural transformation better, the temperature profiles of the reaction were calculated. It has already been reported that the temperature of the melt pool increased with the increase in niobium content. Using the heat equation (m× ρ× ΔT) and the data reported in Table 1, the temperatures of these "endothermic reactions" were calculated and reported in Table 4. Note that the specific heat of 0.61 J/g K at 25 °C [18] was used.

Table 4. Temperature values.

Alloy	Nb (at. %)	Temperature (°C)	Microstructure
BA	0	−253	(α_2 + γ) thick laths of α_2 lamellar
TC	6	−211	α_2 laths → β-precipitates
TB	8	−209	α_2 laths → α_2 + γ grain lamellae
TA	10	−192	α_2 laths → refined lamellar

Table 4 summarises that the temperature of the process increased with the addition of niobium, as anticipated from experimental observations. The binary alloy is highly exothermic; hence, it was intensely cracked [18,19]. Ternary alloy (TA) does not have a greater loss of heat energy when compared to TB and TC. It is endothermic when compared to all other alloys. The retained energy, or minimal loss of the energy to the environment, must be the one leading to the melting and refinement of the microstructure to be fully lamellar. The reaction of Nb to Ti–Al is similar to self-propagating high-temperature synthesis reactions (SHS), which are initiated with sufficient energy being released from the reactants to the products until the reaction is completed. In a handbook of *Non-Ferrous Metal Powders* (second edition), 2019, SHS or combustion synthesis processes, are said to have existed over three decades ago and are necessary for the preparation of intermetallics and composite materials. It was explained that the process is self-sustainable, consumes low energy, and, due to its simplicity and low cost, can be used for short production cycles. In a chapter by H. Peng on the weldability of intermetallics in the same handbook, it was captured that while there is hot cracking and dissimilarity in microstructure between the heat affected zone and the matrix that reduces the mechanical strength of the weld, with solid-state welding (SHS process), such defects can be avoided [20].

The temperature calculations in Table 4 can be read in association with the dissolved aluminium in the alloy (Table 3). It appears that the least exothermic reaction (towards endothermic) leads to the least amount of aluminium being retained in the alloy. This is a consistent observation in the additive manufacturing of Ti–Al alloys. AM processes that are sustained with high energy (in our case, retained heat) lead to the vaporisation of aluminium in the γ + α_2 phase alloys. The results of aluminium dissolution and self-heat generation during alloying Nb to Ti48Al (at. %) alloy are summarised in Figure 6, where it is seen that niobium solubility leads to a high melt-pool temperature and a decrease in aluminium solubility.

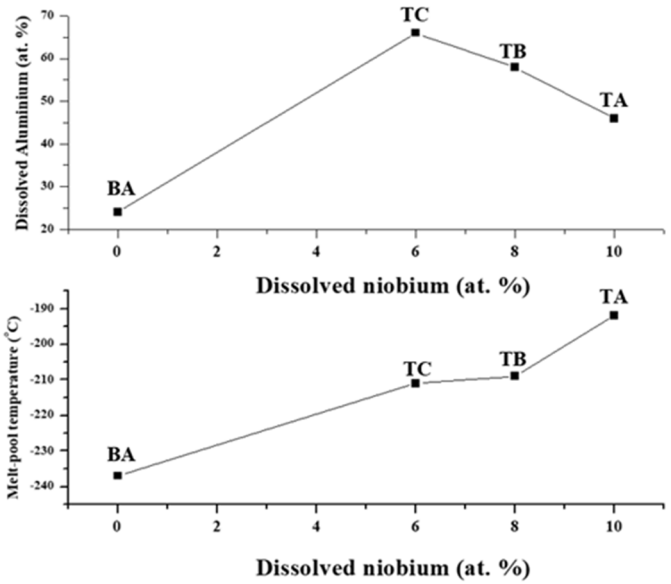

Figure 6. Stacked graph showing the effects of niobium on aluminium solubility (**top**) and heat loss (**bottom**).

After conducting the above experiments, it was pertinent to delve deeper into the findings using the numerical modelling approach. Tlotleng, 2019 [10] and Guangyu et al., 2016 [21] stated that a single deposited unit length of printed product, subjected to laser power, experiences melting and solidification twice during printing. The initial melting and solidification are experienced when the unit length is deposited from the nozzle, and the second melting and solidification are experienced when another unit length is deposited on top of the previously deposited unit length (x). This is experienced repeatedly by subsequent layers until the intended build (in this paper, a cube) is completed. This process of re-melting is accounted for by the thermal conductivity of the intermetallic alloys, which allows for the conduction of adequate heat energy from the melt pool to be transferred to the previously deposited layer during deposition [10,21]. The total thermal energy transferred from the laser to a single unit length of deposited length is displayed in Equation (1):

$$\Delta H = 2.304 \times LEPUL, \tag{1}$$

where *LEPUL* is the Laser Energy Per Unit Length [22]. The *LEPUL* was calculated using Equation (2):

$$Laser\ Energy\ Density\left(\frac{\mathrm{J}}{\mathrm{mm}^2}\right) \times Spotsize(\mathrm{mm}) = LEPUL\left(\frac{\mathrm{J}}{\mathrm{mm}}\right). \tag{2}$$

In addition, the total amount of heat energy absorbed by a single deposited unit length during LENS deposition is the product of the integral of the specific heat with respect to temperature speed and the moles of *Ti* and *Nb* in the resultant phases. The moles of *Ti* and *Nb* are used since *Ti* is a base metal with a high melting temperature, and *Nb* had the highest melting point temperature among all elements used in this study. Thus, the minimum energy required to facilitate the melting of deposited metal powders must be high enough to melt *Ti* and *Nb* powder [23,24]. Heat energy can be calculated as displayed in Equations (3) and (4):

$$\Delta H = n_{Ti} \times C_p \Delta T, \tag{3}$$

$$\Delta H = n_{TiNb} \times C_p \Delta T, \tag{4}$$

Heat energy can also be calculated as displayed in Equations (5) and (6):

$$\Delta H = n_{Ti} \times \int_{298}^{T_M} C_p dT, \tag{5}$$

$$\Delta H = n_{TiNb} \times \int_{298}^{T_M} C_p dT, \tag{6}$$

where n is the total amount of *Ti* and *Nb* moles [23] in the build, C_p is the specific heat (J/mol-K), and T is the temperature velocity (K/cm) since the deposition nozzle moves at a velocity [23,25]. The temperature values of the specific heat C_p for various phases are displayed in Table 5.

Table 5. Specific heat values for various phases with respect to temperature.

C_P (T)	Temperature Range (K)	References
$C_{P(Ti,l)} = 11.042$ (J/mol-K)	1943	[26,27]
$C_{P(Ti,\gamma)} = 47.32 + 5.568 \times 10^{-3}T - 1.549 \times 10^{-5}T^2 + 2.223 \times 10^{-8}T^3$ (J/g-K)	673–1703	[28]

The Equations listed in Table 5 were substituted into Equations (7) and (8). This was performed to calculate the unknown solidification temperature velocities depicted as T_S (K/cm) [23,29]. The values for T_S were obtained in Microsoft EXCEL using SOLVER. Below are the equations used to solve for T_S:

For various builds, T_S is obtained by solving Equations (7) and (8) for T_S.

$$\Delta H = n_{Ti}\left[\int_{T_S}^{T_L} \frac{C_{p(Ti,l)}}{M_{Ti}} dT + \int_{298}^{T_S} C_{p(TiAlNb,\gamma)} dT\right], \tag{7}$$

$$\Delta H = n_{TiNb}\left[\int_{T_S}^{T_L} \frac{C_{p(Ti,l)}}{M_{TiNb}} dT + \int_{298}^{T_S} C_{p(TiAlNb,\gamma)} dT\right], \tag{8}$$

where M depicts molar mass, which allows for unit conversion during calculation.

It was assumed that the minimum temperature required from the laser should be high enough to melt *Ti* and *Nb* powders; thus, T_M = 1943 K and 2742 K [30] were used. Values obtained for T_S allowed for the calculation of the cooling rates per unit length during deposition until solidification was complete.

The thermal gradient of a singularly deposited unit length until the completion of solidification with respect to time is displayed in Equation (9) as the derivative of temperature with respect to time that is inversely proportional to cooling rates and solidification rates as displayed in Equation (10) [25].

$$\frac{\partial T}{\partial t} = \frac{|T_M - T_S|}{t_M - t_S} = \frac{|T_M - T_S|}{\Delta t} \alpha \frac{1}{cooling\ rates} \tag{9}$$

$$R = \frac{1}{G}\frac{\partial T}{\partial t} \tag{10}$$

The thermal gradient with respect to unit length deposited can be expressed as a derivative of temperature with respect to unit length Δx as displayed in Equation (11).

$$\frac{dT}{dx} = \frac{|T_M - T_S|}{\Delta x} \tag{11}$$

Figure 7 displays thermal gradients with respect to Ti. It is observed that for the binary alloy (BA), *dT/dx* decreases as LEPUL increases, which is indicative of increased cooling rates (rapid cooling); hence, the cube built was intensely cracked [18]. However, on *Nb* addition at low *LEPUL*, *dT/dx* remains high. As *Nb* (at. %) increases, *dT/dx* values

become negative, which indicates an increase in T_S to values higher than $T_{M(Ti)}$. This means there is increased heating due to exothermic reactions resulting from Nb addition. These exothermic reactions heat up the melt pool and increase the solidification temperature velocities prior to cooling and γ phase formation. This means slower cooling rates are observed as *Nb* is increased. The enhancement of the red glow as *Nb* (at. %) and LEPUL increase is credited to the increased T_S with respect to *Ti*.

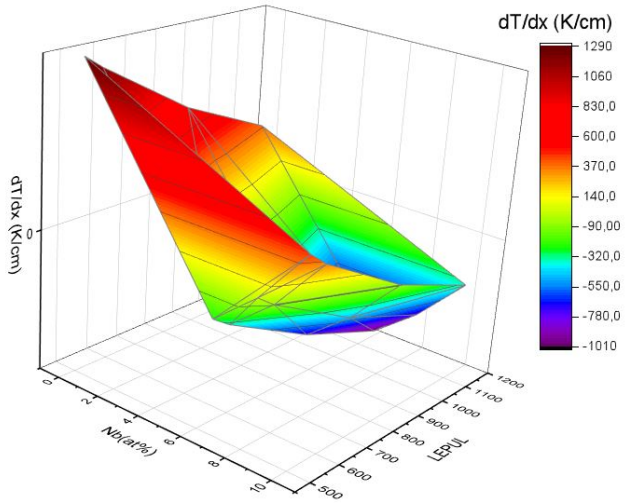

Figure 7. The effects of LEPUL and Nb (at. %) on thermal gradients with respect to Ti.

Figure 8 shows thermal gradients with respect to TiNb. It is observed that the addition of Nb in small amounts 6 (at. %) leads to negative dT/dx, which results in heating of the melt pool. However, as Nb (at. %) increases with LEPUL, high dT/dL are yielded, which indicates slower cooling rates during deposition. This means that the exothermic reactions supply heat to facilitate endothermic processes, which allow for slow cooling to occur.

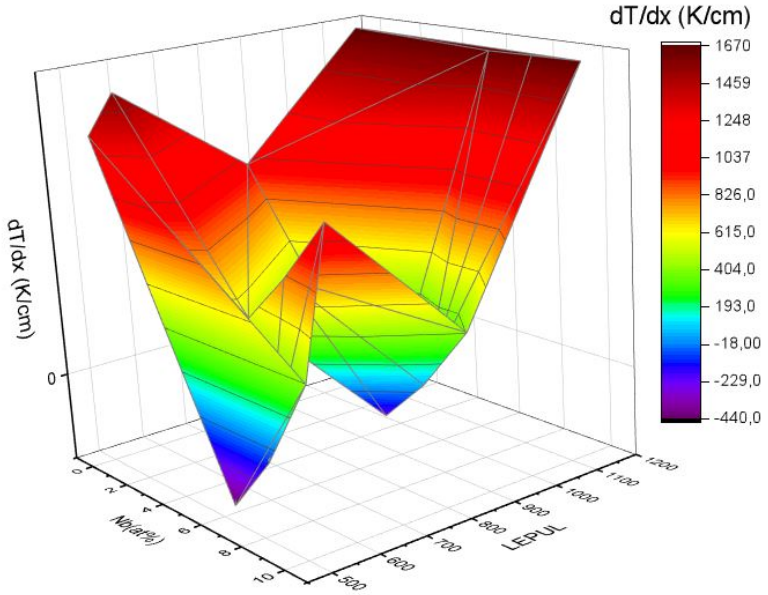

Figure 8. The effects of LEPUL and Nb (at. %) on thermal gradients with respect to TiNb.

3.1. Twinning in the As-Built Samples

Niobium can promote the solubility of aluminium and anneal twinning in the γ-TiAl alloys. The diffractograph of the as-built samples shown in Figure 9 discusses the twinning formation in the alloys.

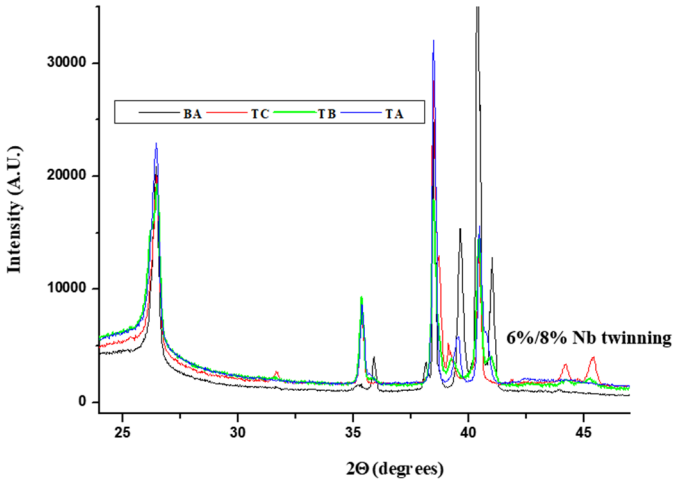

Figure 9. Twinning in the Ti–Al/Nb alloys.

Figure 9 shows the dissolution of the aluminium lean phases (α_2) at 2θ peak position range of 39–41° and the preservation of the γ-phase with the addition of niobium. Meanwhile, twinning was absent in the binary phase alloy and the ternary alloys containing Nb of 8–10 (at. %). Perfect twinning was observed for the sample that contained 6 (at. %) Nb and was identified as α_2 twins. These twins were destroyed when 8 (at. %) Nb was added and completely diminished in the alloy that contained 10 (at. %) Nb.

The observed twinning in the as-built sample that contains 6 (at. %) Nb alloy could not be explained as it has not been reported before. However, it may be attributed to the dissolution ability of aluminium with niobium in the dual phase alloys, which is hindered in the pure γ phase alloys. The Al_2O_3 peak (2θ of 26°) is present in all samples. There are no pure peaks of niobium that can be identified on the spectrum; this indicates that it was fully alloyed into the matrix of the binary Ti–Al alloy. The effect of annealing on the twining of these alloys is reported next.

3.2. Twinning in Annealed Conditions

3.2.1. Condition 1: Annealing Twinning in the Binary Samples

Hashimoto et al. proposed that Nb, when added to the γ-TiAl alloy, will lead to twinning in the annealing condition. To ascertain this proposal, the microstructures of the alloys post-annealing and the corresponding XRD graphs are reported in Figures 10–15, respectively, for Condition 1 (1200 °C) and Condition 2 (1400 °C). Figure 10 presents the effects of heat treatment on twinning in the binary alloy. The peaks were assigned using these reference codes: $TiAl_3$ (00-026-0038), TiAl (00-005-0678), Ti_3Al (00-052-0859), Al_2O_3 (00-004-0877), TiO_2 (00-015-0875), Cubic Pm-3m (04-016-6790), hexagonal (P63/mmc), Orthorhombic (04-017-6137), and $TiAlNbO_2$ (01-088-1981).

Figure 10 shows explicitly that not only does heat treatment promote homogenisation in this alloy, but it also dissolves the unstable α_2 phase, leading to a stable pure γ phase alloy. No twinning was observed for the alloy after heat treatment at 1400 °C. Perfect twins of the α_2 phase are observed after heat treatment at 1200 °C at 2θ positions of 40.255° and 40.754°. An intense peak (2θ of 26.442°) was observed post-heat treatment at 1200 °C that corresponds to the titanium oxide (TiO_2) phase, which is absent in the as-built and samples that were heat treated at 1400 °C. The as-built sample and the sample that was heat treated to 1400 °C have an oxide layer present at the 2θ peak position of 39.677° that corresponds to the Al_2O_3 phase. Overall, this XRD spectrum concludes that the as-built alloy was a dual phase alloy (α_2 +γ), where α_2 phase was the figure print of the alloy, and after heat treatment the aluminium-rich phase (α_2) was dissolved, leading to the alloy where γ phase was the figure print, as seen from Figure 11, which reports the SEM images of the alloys post-heat treatment.

Figure 11 presents the near lamellar and fully lamellar microstructures of the binary alloy post-heat treatment at 1200 °C and 1400 °C, respectively. These SEM images validate that the binary alloy post-heat treatment at 1400 °C was dual phase (α_2 + γ) in γ with dislocation pile-up present in the α_2 while the γ just experienced dislocation motion. No twinning was observed in this alloy. Primary and secondary dislocation planes and a few dislocation pile-ups were observed in the sample heat-treated to 1200 °C. The dark phase is typically γ, while the bright phase is typically indexed α_2 in Ti–Al research. It can simply be concluded that, indeed, twinning was present in the α_2 phase in this alloy as per the XRD data. Twinning in the ternary alloys is studied next in Conditions 2 and 3 for 1200 °C and 1400 °C, respectively.

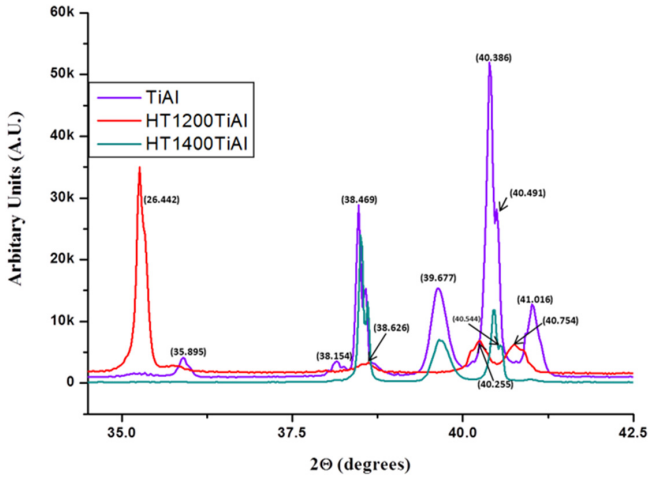

Figure 10. Anneal twinning in the binary alloy.

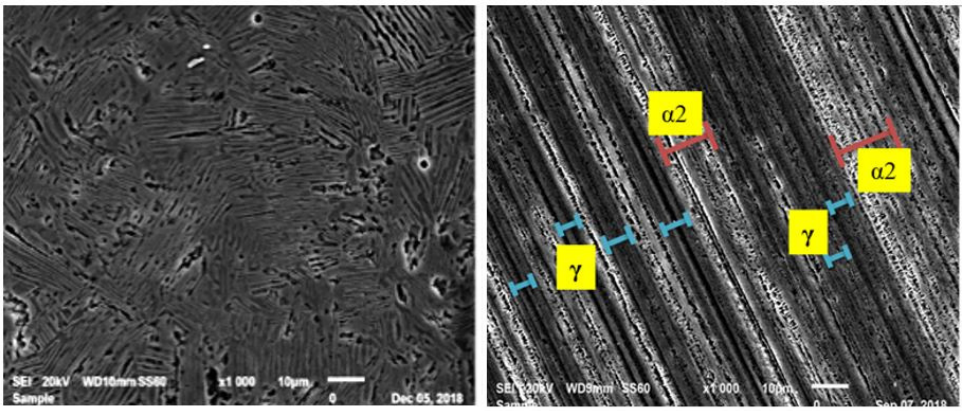

Figure 11. SEM microstructure of the heat treated: 1200 (**left**) and 1400 (**right**) samples.

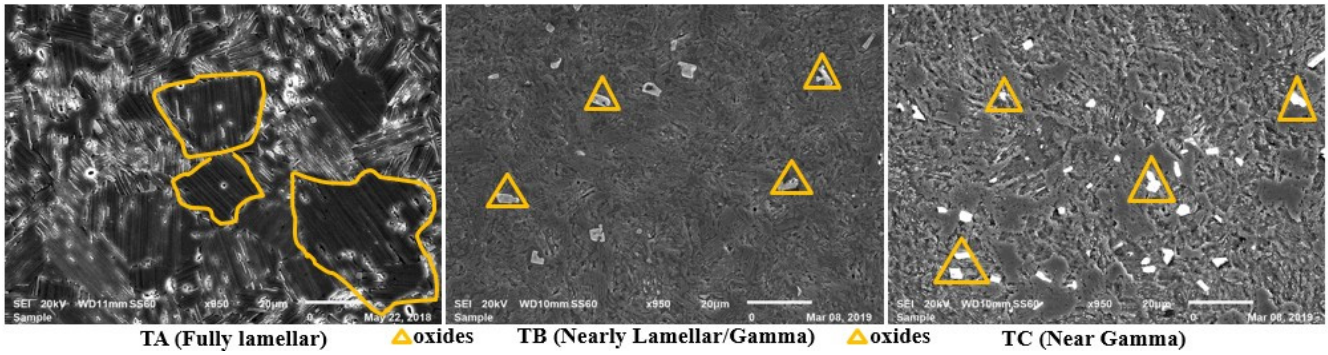

Figure 12. Microstructural evolution with heat treatment at 1200 °C.

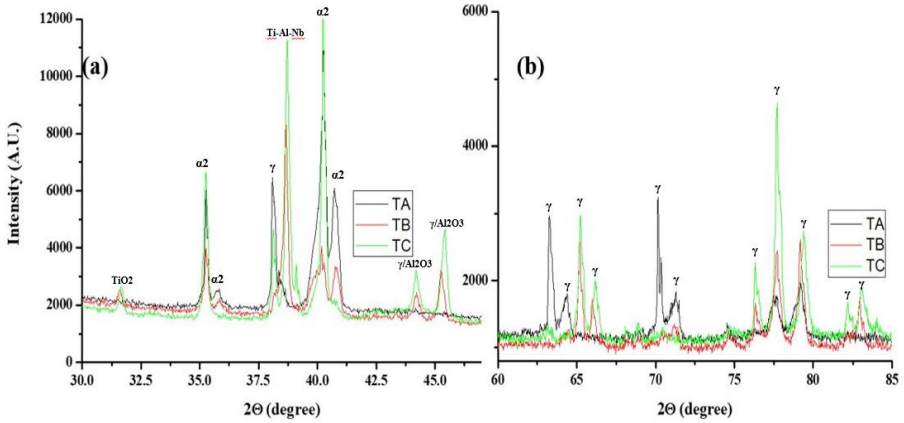

Figure 13. XRD plots of TiAl–Nb after heat treatment at 1200, lower (**a**) and higher (**b**) 2Θ values.

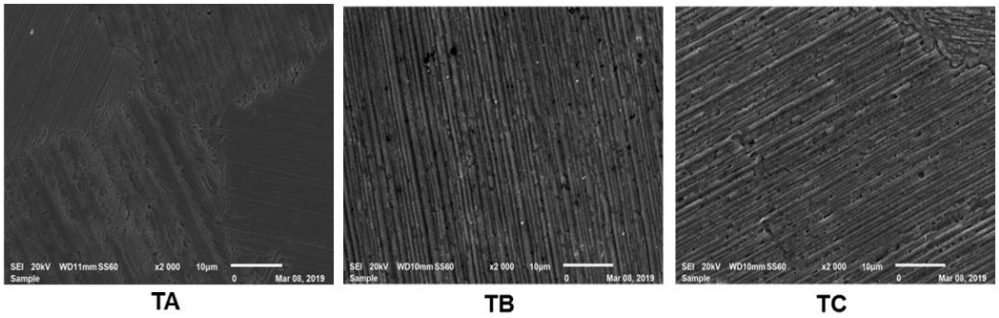

Figure 14. Twinning in the annealing condition is only possible at 1400 °C.

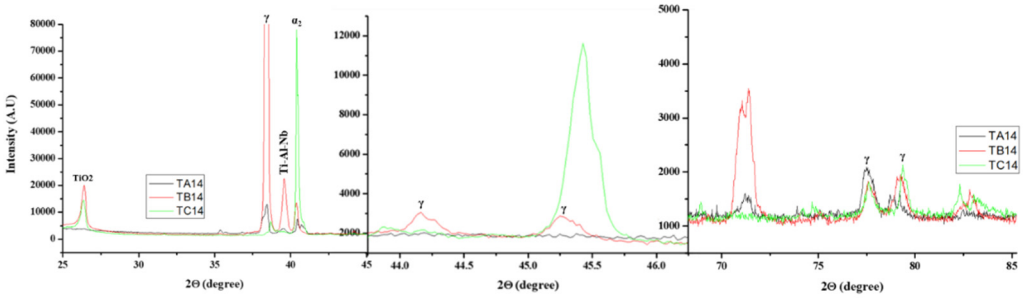

Figure 15. Twinning in an annealing condition (HT 1400 °C).

3.2.2. Condition 2: Heat Treatment at 1200 °C

Figure 12 reports the microstructures of the ternary alloys after heat treatment at 1200 °C and furnace cooling in an argon environment.

The microstructures are identified as near gamma for the alloy containing 6% Nb (TC), nearly lamellar/gamma for the alloy containing 8% Nb (TB), and fully lamellar for the alloy containing 10% Nb (TA). The Al_2O_3 particles, indicated by a circle (O) on the microstructure, are present in all the ternary alloys except for the alloy that contained 10% Nb (TA), which serves as an indication that the latter alloy was oxidation resistant. There exists no perfect γ anneal twinning in the 10% Nb alloy (TA), and the γ phase lamellar highlighted experienced no dislocation pile-up, but dislocation rapture terminated and continued to form α_2 phase lamellar structures. Dislocation pile-ups are experienced by the α_2 phase in this alloy. Similarly, an alloy containing 8% Nb, even though it did not experience any dislocation motion, cannot be said to have twinning present. No twinning or dislocations are expected for the near gamma alloy (TC). The XRD plots of these alloys are reported in Figure 13.

The XRD spectrum shows no signs of anneal twinning. There are three peaks in the 2θ region of 76–79.8°, which correspond to the γ phase. A shift towards the low 2θ values,

from 65 to 66° in the TB and TC alloys to 63 to 65° in the alloy that contained 10% Nb (TA), can be observed. Normally, the shift in the crystal's structure can be an indication of atomic rearrangement. These two peaks correspond to the γ phase peak. A cubic (Pm-3m) Ti–Al–Nb phase is a major peak for the TB alloy only and a second most intense peak for the TA and TC alloys, which happened to have α_2 as their major peak. Both TC and TB alloys have a TiO_2 phase that is absent in the TA alloy. Likewise, the γ/Al_2O_3 phase is absent in the TA alloy and present in the TA and TB alloys. These two phases, TiO_2 and γ/Al_2O_3, seem to decrease in intensity with the addition of Nb to a point of diminishing in the TA alloy that has a higher Nb content. The observation of the oxide phase in the TB and TC alloys is supported by the SEM images of the alloys, which are presented in Figure 12. Additionally, the observation that the TC alloy was near gamma is corroborated by the XRD data, as this alloy is missing the γ peak (2θ of 38°) as one of the intense peaks. Unfortunately, these alloys are missing the anticipated anneal twins, leading to the conclusion that 1200 °C did not promote twinning in the Ti–Al–Nb alloy system. Further investigation on anneal twinning is discussed next in Condition 3.

3.2.3. Condition 3: Heat Treatment at 1400 °C

Microstructure and XRD data of the samples after heat treatment at 1400 °C and furnace cooling are reported in Figures 14 and 15.

Figure 14 presents the microstructures of the alloys post-heat treatment at 1400 °C. A well-aligned and spaced lamellar structure was observed for the binary phase alloy that alternates between the γ and α_2 clearly marked. A perfect γ-twinned, micron-spaced lamellar (TB) and lamellae (TC) are observed for the lower Nb content (TB and TC). This twinning and spacing is not perfect in the higher Nb content (TA), where agglomeration, lamellar thickening, and dislocations in the α_2 phase and grain boundary were prevalent. However, the spacing in the lamellar and alternates of γ and α_2 are easily observed. This might suggest that there is not a perfect twinning in the alloy that contains Nb of 10 (at. %) in the α_2 phase but could exist in the γ phase. Generally, perfect refinement and alignment in the lamellar can be concluded for TB and TC, with dislocations present in both samples and pile up in the α_2 phase of the TA sample. It is anticipated that 1400 °C, as opposed to 1200 °C, led to anneal twinning in all the alloys. The XRD plots of the samples are reported in Figure 15.

Figure 15 reports the XRD spectrum of the ternary alloy after heat treatment at 1400 °C. A cubic (Pm-3m) phase is present in all the samples but intense in the TB alloy, which contains 8% Nb. The γ phase is the intense peak for both the TA and TB alloys, while α_2 phase is the major peak for the TC alloy. This is acceptable and corroborates the information reported in Table 3, where TA and TB had aluminium content >49%, making them pure gamma alloys, while TC had aluminium content $\leq$49%, making it a dual phase gamma alloy. In the 1200 °C heat-treated alloy, the TiO_2 phase is absent in the alloy with high niobium content (TA) and present in TB and TC alloys. In fact, no oxide phase can be reported for the TA alloy, making it an oxidation-resistant alloy at high temperatures. Anneal twinning in the γ phase was only observed to be present in the alloy that contained 8 (at. %) Nb (TB alloy). This observation indicates that Nb promotes anneal twinning at temperatures of about 1400 °C but not at 1200 °C when 8 (at. %) Nb is added to the Ti–48%Al alloy.

4. Conclusions

This paper presents a study concerning the laser in situ alloying of Ti–Al–Nb using the LENS technique. The objectives were to elucidate the effects of niobium on the structure of gamma Ti–48Al alloy. From the results and discussion of this study, the following was concluded:

- Niobium increases and decreases the aluminium solubility in the dual (α_2 + γ) and pure γ phase alloys, respectively.

- Niobium had a direct microstructural transformation effect on the Ti–48Al alloy. This microstructural transformation was attributed to the resulting exothermic reaction, which is also known as a self-propagating high-temperature synthesis or combustion synthesis.
- Niobium 6 (at. %) promotes twinning in α_2 phase for Ti–48Al alloy, while anneal twinning in the gamma (γ) phase can be achieved for the sample containing 8 (at. %) niobium content if heat treated to 1400 °C and oven cooled.

5. Outlook: The Benefits of Additive Manufacturing

Three-dimensional printing or additive manufacturing of metallic components is aimed at improving the efficiency of the production of complex components that are durable and expensive, which could not necessarily be accomplished with traditional forging and casting machinery. This advent presents an opportunity for industries and small, micro, and medium enterprises (SMMEs) to realise a full value chain in metal alloy production and processing in the most cost-effective sense. Until the need for lightweight frames and component structures in aeroplanes, the industry of metal 3D printing was performing adequately. With the understanding that the intermetallic group of alloys, called titanium aluminides, presents the potential for durable lighter structures, 3D printing of aerospace structures was centred on Grade 5 titanium alloy (Ti6Al4V); hence, there are so many scientific articles on the topic of additive manufacturing or 3D printing of Ti6Al4V.

According to the MarketWatch news report of 5 November 2019, the titanium aluminide market was valued at 140M USD in 2018 and is expected to reach a market share of 640M USD, a growth rate of about 21% in the period of 2019–2025. To share in this wealth, many big corporations and industries have embarked on understanding how the route to alloy development, processing, and part printing can be achieved. The success of Boeing in manufacturing Ti–Al components for Boeing's Dreamliner 747-8 aircraft and Boeing's next-generation long-haul plane (the 777X) is the greatest achievement, however exorbitant in set-up and post-processing.

To advance further in manufacturing, aircraft companies would be in search of functionally graded structures that can serve in different environments and adapt without failing, and this need cannot immediately be met with powder bed technologies. These structures can only be achieved with direct energy deposition technologies, given their freedom of operation and powder deposition. Many FGM studies have been commissioned on the characteristic change (improvement) of one powder over the other. However, the use of similar approaches in powder alloy development in flight during 3D printing was not yet commissioned until around 2015–2018. Until recently, studies using the alloy approach in Ti–Al research have achieved crack-free builds. Of greatest importance are the remarkable results achieved by laser metal in situ alloying during 3D printing. There are those who have predicted a cost savings of up to 40% in material cost reduction when 3D printing Ti–Al from its elemental powders. Therefore, this study contributes to the industry by providing a process for making Ti–Al–Nb alloys that could be machined, leading to cost savings.

With respect to saving costs during manufacturing, in a handbook of *Non-Ferrous Metal Powders* (second edition), 2019, three chapters were of significance to be reviewed and captured as a summary in this work. The authors put into context the benefits of the self-propagating process (or SHS), with a particular focus on Ti–Al.

6. Patents

A patent for this work is not yet registered, but aspects of it will be patentable in the future. The aspects to be patented are as follows:

1. The use of a laser beam as a melting pot to produce alloys from single-phase metals during laser metal additive manufacturing makes use of the in situ alloying methodology/approach that the researchers at the CSIR, South Africa, have developed, optimised, and published.

2. The use of niobium [6 or 8 (at. %)] to promote or induce twinning or anneal twining in gamma Ti–48Al alloys and achieve the SHS synthetic process.

Author Contributions: Writing—original draft preparation by M.T. and S.M.; funding acquisition by S.P. and M.T. All authors have read and agreed to the published version of the manuscript.

Funding: This research was funded by the Council for Scientific and Industrial Research (CSIR; Thematic Projects Number: LMTRAC) and the National Research Foundation (NRF), Thuthuka Grant Number: TTK160527166453.

Institutional Review Board Statement: Not applicable for this study.

Informed Consent Statement: Not applicable for this study.

Data Availability Statement: All data is kept on the drives of the depository of the Council for Scientific and Industrial Research.

Acknowledgments: The authors would like to acknowledge: (1) The CSIR and NRF for their funding. (2) My colleagues, Nana Arthur, Samuel Skosane, Bathusile Masina, Sadiq A. Raji, Lehlogonolo Kanyane, and Paul Lekoadi, for the interest they showed in this study.

Conflicts of Interest: The authors declare no conflict of interest.

References

1. Herzog, D.; Seyda, V.; Wycisk, E.; Emmelmann, C. Additive manufacturing of metals. *Acta Mater.* **2016**, *117*, 371–392. [CrossRef]
2. DebRoy, T.; Wei, H.L.; Zuback, J.S.; Mukherjee, T.; Elmer, J.W.; Milewski, J.O.; Beese, A.M.; Wilson-Heid, A.; De, A.; Zhang, W. Additive manufacturing of metallic components–process, structure and properties. *Prog. Mater. Sci.* **2018**, *92*, 112–224. [CrossRef]
3. Tlotleng, M.; Pityana, S. LENS manufactured γ-TNB turbine blade using Laser "In Situ" alloying approach. *MRS Adv.* **2020**, *5*, 1203–1213. [CrossRef]
4. Sharman, A.; Hughes, J.; Ridgway, K. Characterisation of titanium aluminide components manufactured by laser metal deposition. *Intermetallics* **2018**, *93*, 89–92. [CrossRef]
5. Shishkovsky, I.; Missemer, F.; Smurov, I. Direct metal deposition of functional graded structures in Ti-Al system. *Phys. Procedia* **2012**, *39*, 382–391. [CrossRef]
6. Wang, G.-X.; Bartels, A.; Dahms, M. Influence of heat treatment on microstructure and deformation behaviour of the Alloy Ti50Al48Cr2 prepared by reactive powder processing. *Mater. Trans. JIM* **1993**, *34*, 228–235. [CrossRef]
7. Ma, Y.; Cuiuri, D.; Hoye, N.; Li, H.; Pan, Z. Characterization of in-situ alloyed and additively manufactured titanium aluminides. *Metall. Mater. Trans. B* **2014**, *45*, 2299–2303. [CrossRef]
8. Balla, V.K.; Das, M.; Mohammad, A.; Al-Ahmari, A.M. Additive Manufacturing of γ-TiAl: Processing, Microstructure, and Properties. *Adv. Eng. Mater.* **2016**, *18*, 1208–1215. [CrossRef]
9. Appel, F.; Oehring, M.; Paul, J. A novel in situ composite structure in TiAl alloys. *Mater. Sci. Eng. A* **2008**, *493*, 232–236. [CrossRef]
10. Tlotleng, M. Microstructural properties of heat-treated LENS in situ additively manufactured titanium aluminide. *J. Mater. Eng. Perform.* **2019**, *28*, 701–708. [CrossRef]
11. Nochovnaya, N.; Panin, P.; Kochetkov, A.; Bokov, K. Modern refractory alloys based on titanium gamma-aluminide: Prospects of development and application. *Met. Sci. Heat Treat.* **2014**, *56*, 364–367. [CrossRef]
12. Clemens, H.; Bartels, A.; Bystrzanowski, S.; Chladil, H.; Leitner, H.; Dehm, G.; Gerling, R.; Schimansky, F.P. Grain refinement in γ-TiAl-based alloys by solid state phase transformations. *Intermetallics* **2006**, *14*, 1380–1385. [CrossRef]
13. Kesler, M.S.; Goyel, S.; Ebrahimi, F.; Manuel, M.V. Effect of microstructural parameters on the mechanical behavior of TiAlNb (Cr, Mo) alloys with γ+ σ microstructure at ambient temperature. *J. Alloys Compd.* **2017**, *695*, 2672–2681. [CrossRef]
14. Yoshihara, M.; Miura, K. Effects of Nb addition on oxidation behavior of TiAl. *Intermetallics* **1995**, *3*, 357–363. [CrossRef]
15. Hashimoto, K.; Doi, H.; Kasahara, K.; Nakano, O.; Tsujimoto, T.; Suzuki, T. Effects of additional elements on mechanical properties of TiAl-based alloys. *J. Japan Inst. Met.* **1988**, *52*, 1159–1166. [CrossRef]
16. Kawabata, T.; Fukai, H.; Izumi, O. Effect of ternary additions on mechanical properties of TiAl. *Acta Mater.* **1998**, *46*, 2185–2194. [CrossRef]
17. Kothari, K.; Radhakrishnan, R.; Wereley, N.M. Advances in gamma titanium aluminides and their manufacturing techniques. *Prog. Aerosp. Sci.* **2012**, *55*, 1–16. [CrossRef]
18. Balichakra, M.; Bontha, S.; Krishna, P.; Balla, V.K. Prediction and validation of residual stresses generated during laser metal deposition of γ titanium aluminide thin wall structures. *Mater. Res. Express* **2019**, *6*, 106550. [CrossRef]
19. Kenel, C.; Dasargyri, G.; Bauer, T.; Colella, A.; Spierings, A.B.; Leinenbach, C.; Wegener, K. Selective laser melting of an oxide dispersion strengthened (ODS) γ-TiAl alloy towards production of complex structures. *Mater. Des.* **2017**, *134*, 81–90. [CrossRef]
20. Naboynchenko, S.S.; Yefimov, N.A. *Handbook of Non-Ferrous Metal Powders: Technologies and Applications*, 2nd ed.; Neikov, O.D., Ed.; Elsevier: Moscow, Russia, 2019.

21. Yang, G.; Jia, W.; Zhao, P.; Jia, L.; Liu, N.; Wang, J.; Tang, H. Microstructures of as-fabricated and post heat treated Ti-47Al-2Nb-2Cr alloy produced by selective electron beam melting (SEBM). *Rare Met. Mater. Eng.* **2016**, *45*, 1683–1686.
22. Gu, D.; Wang, H.; Dai, D.; Chang, F.; Meiners, W.; Hagedorn, Y.-C.; Wissenbach, K.; Kelbassa, I.; Poprawe, R. Densification behavior, microstructure evolution, and wear property of TiC nanoparticle reinforced AlSi10Mg bulk-form nanocomposites prepared by selective laser melting. *J. Laser Appl.* **2015**, *27*, S17003. [CrossRef]
23. Sciammarella, F.M.; Najafabadi, B.S. Processing Parameter DOE for 316L Using Directed Energy Deposition. *J. Manuf. Mater. Process.* **2018**, *2*, 61. [CrossRef]
24. Valencia, J.J.; Quested, P.N. Thermophysical Properties. In *Casting: ASM Handbook*; ASM: Novelty, OH, USA, 2013.
25. Bontha, S.; Klingbeil, N.W.; Kobryn, P.A.; Fraser, H.L. Thermal process maps for predicting solidification microstructure in laser fabrication of thin-wall structures. *J. Mater. Process. Technol.* **2006**, *178*, 135–142. [CrossRef]
26. Mills, K.C. *Recommended Values of Thermophysical Properties for Selected Commercial Alloys*; Woodhead Publishing: Sawston, UK, 2002.
27. Smithells, C.J.; Brandes, E.A. *Smithells Metals Reference Book*; Butterworth-Heinemann: Oxford, UK, 1992.
28. Egry, I.; Brooks, R.; Holland-Moritz, D.; Novakovic, R.; Matsushita, T.; Ricci, E.; Seetharaman, S.; Wunderlich, R. Thermophysical properties of γ-titanium aluminide: The European IMPRESS project. *Int. J. Thermophys.* **2007**, *28*, 1026–1036. [CrossRef]
29. Zheng, B.; Zhou, Y.; Smugeresky, J.; Schoenung, J.; Lavernia, E. Thermal behavior and microstructural evolution during laser deposition with laser-engineered net shaping: Part I. Numerical calculations. *Metall. Mater. Trans. A* **2008**, *39*, 2228–2236. [CrossRef]
30. Schuster, J.C.; Palm, M. Reassessment of the binary aluminum-titanium phase diagram. *J. Phase Equilibria Diffus.* **2006**, *27*, 255–277. [CrossRef]